On the Product of Two κ–μ Random Variables and its Application to Double and Composite Fading Channels

Nidhi Bhargav, *Student Member, IEEE*, Carlos Rafael Nogueira da Silva, Young Jin Chun, *Member, IEEE*, Élvio João Leonardo, Simon L. Cotton, *Senior Member, IEEE*, and Michel Daoud Yacoub, *Member, IEEE*

***Abstract*— In this paper, we perform a systematic investigation of the statistics associated with the product of two independent and non-identically distributed κ–μ random variables. More specifically, we develop novel analytical formulations for many of the fundamental statistics of interest, namely, the probability density function, cumulative distribution function, and moment-generating function. Using these new results, closed-form expressions are obtained for the higher order moments, amount of fading and channel quality estimation index, while analytical formulations are obtained for the outage probability, average channel capacity, average symbol error probability, and average bit error probability. These general expressions can be reduced to a number of fading scenarios, such as the double Rayleigh, double Rice, double Nakagami-*m*, κ–μ/Nakagami-*m*, and Rice/Nakagami-*m*, which all occur as special cases. Additionally, as a byproduct of the work performed here, formulations for the κ–μ/κ–μ composite fading model can also be deduced. To illustrate the efficacy of the novel expressions proposed here, we provide useful insights into the outage probability of a dual-hop system used in body area networks, and demonstrate the suitability of the κ–μ/κ–μ composite fading for characterizing shadowed fading in device-to-device channels.**

***Index Terms*— composite fading channels, device-to-device channels, κ-μ fading, multi-hop relay, multipath fading, product distribution, shadowing.**

I. Introduction

THE product of random variables (RVs) is of great importance as it finds application in a broad range of wireless communication systems. For instance, in cascaded fading channels and keyhole channels of multiple-input-multiple-output (MIMO) systems [1], where the received signal is treated as a product of random variables (RVs). Another application area is that of backscatter communications such as those found in radio frequency identification (RFID) systems. Here, the channel from the reader to the tag, and the tag to the reader can be viewed as a product of RVs [2]–[5]. These channels were modeled using the product of Rayleigh RVs in [2] and [3]. Furthermore, [4] studied point-to-point backscatter communications where the wireless channel was treated as a product of two Rician RVs (also known as dyadic Rician fading channel), while the work in [5] considered a multiuser setting where the channel from each tag to the reader was modeled as a product of Nakagami-*m* RVs (also known as dyadic Nakagami-*m* fading channel).

Likewise, in dual-hop wireless systems [6] the channel from a source to a destination may be obtained as the product of the RVs that describe each individual hop. Traditionally, the simplest way of modeling such channels is to use the double Rayleigh [7] or the double Rician fading model [8]. For these cases, analytical expressions have been obtained for the main statistical properties such as the probability density function (PDF), cumulative distribution function (CDF), mean and variance in [7] and [8]. Previous work on the characterization of keyhole channels in MIMO systems using the double Rayeigh fading model was conducted in [9]. This work was later extended to consider the double Nakagami-*m* model in [10].

The double fading model also represents *worse than Rayleigh* fading statistics as can be seen in [11]. As well as this, it has been used to characterise atmospheric turbulence in wireless optical communications, where it was shown to provide an excellent fit with the measured data [12], [13]. Hence, the application of the double fading model goes well beyond characterizing RF wireless channels. More general approaches have been considered where the received signal is formed from the product of N cascaded fading channels. Specifically, [14] and [15] provided theoretical results for the case of $N\times$Rayleigh and $N\times$Nakagami-*m* channels, respectively. More recently, exact closed-form expressions were presented in [16] for the PDF and CDF of the product of an arbitrary number of α-μ RVs.

Manuscript received June 20, 2017; revised November 16, 2017 and January 4, 2018; accepted January 8, 2018. Date of publication January 26, 2018; date of current version April 8, 2018. This work was supported in part by the U.K. Engineering and Physical Sciences Research Council under Grant EP/L026074/1, in part by the Department for the Economy Northern Ireland under Grant USI080, and in part by CNPq under Grant 304248/2014-2. The associate editor coordinating the review of this paper and approving it for publication was M. Elkashlan. *(Corresponding author: Simon L. Cotton.)*

N. Bhargav, Y. J. Chun, and S. L. Cotton are with the Wireless Communications Laboratory, Institute of Electronics, Communications and Information Technology, Queen's University of Belfast, Belfast BT3 9DT, U.K. (e-mail: nbhargav01@qub.ac.uk; y.chun@qub.ac.uk; simon.cotton@qub.ac.uk).

C. R. N. da Silva and M. D. Yacoub are with the Wireless Technology Laboratory, School of Electrical and Computer Engineering, University of Campinas, 13083-970 Campinas, Brazil (e-mail: carlosrn@decom.fee.unicamp.br; michel@decom.fee.unicamp.br).

É. J. Leonardo is with the Department of Informatics, State University of Maringá, 87020-900 Maringá, Brazil (e-mail: ejleonardo@uem.br).

Color versions of one or more of the figures in this paper are available online at http://ieeexplore.ieee.org.

Digital Object Identifier 10.1109/TWC.2018.2796562

Another key use of the product of RVs is in the computation of composite fading statistics which can be found as a particular case of their statistics [16]. It is well known that wireless communication channels can undergo simultaneous small-scale fading and shadowing [17]. Small-scale fading results from multipath scattering, whereas shadowing is introduced by the topographical elements and objects obstructing the signal path. To model these propagation mechanisms, several statistical distributions have been proposed. For example, popular small-scale fading models include the Rayleigh, Rice, Nakagami-m, Hoyt and Weibull distributions. More recently, generalized statistical distributions such as the κ-μ and η-μ [18] fading models have been considered due to their versatility and the fact that they include the majority of the aforementioned small-scale fading distributions as special cases. On the other hand, shadowing is often modeled using the lognormal [19] or gamma [20] distributions. To encapsulate the concurrent effects of both small-scale fading and shadowing, which are known to occur in wireless applications such as body area networks (BANs) [21], device-to-device (D2D) [22] and vehicle-to-vehicle (V2V) communications [11], several new composite fading models have been proposed [23]. Different from the more established composite fading models such as the K-distribution [24] and generalized K-distribution [25], these models assume that the small-scale fading follows either κ-μ [18] or η-μ [18] distribution while the shadowing is characterized by the inverse gamma distribution.

In this study, we focus our attention on the κ-μ distribution [18] which has been developed to describe channels that may admit the clustering of scattered multipath waves in addition to dominant components. It is described by two physical fading parameters, namely κ and μ. Here, κ represents the ratio of the total power of the dominant components to the total power of the scattered waves whilst μ represents the number of multipath clusters. It is a very general model and contains other important distributions such as the Rice ($\kappa = K$, $\mu = 1$), Nakagami-m ($\kappa \to 0$, $\mu = m$), Rayleigh ($\kappa \to 0$, $\mu = 1$) and One-Sided Gaussian ($\kappa \to 0$, $\mu = 0.5$) as special cases. As a result of its flexibility, it is unsurprising that it yields a very good fit to many practical wireless channels of interest [26].

Motivated by this, in this paper we analyze the product of two independent and non-identically distributed ($i.n.i.d$) κ-μ RVs. Novel analytical expressions for the PDF, CDF and moment-generating function (MGF) are derived. These results are then used to obtain new closed-form expressions for the moments, amount of fading (AF) and channel quality estimation index (CQEI). As well as this, analytical formulations are derived for the outage probability, average channel capacity, average symbol error probability, and average bit error probability of the double κ-μ fading channel. It is worth remarking that these expressions are very flexible and encompass a number of other fading scenarios such as the double Rayleigh, double Rice, double Nakagami-m, double One-Sided Gaussian and product mixtures of these fading models as special cases. Since the composite fading statistics can be found as a special case of the statistics of the product of RVs, the results derived here can also be used to describe κ-μ/κ-μ composite fading conditions. Here, the small-scale fading is described by a κ-μ distribution whose mean (i.e. the shadowing) follows another κ-μ distribution. Thus, the expressions presented here also encompass a number of other composite fading scenarios as special cases. Some examples include κ-μ/Nakagami-m, Rice/Nakagami-m, and Rayleigh/Nakagami-m. Finally, we illustrate the utility of these new results by estimating the outage probability of a dual-hop body area network (BAN) system, and then applying the κ-μ/κ-μ composite fading model to some D2D channel measurements.

It should be noted that the product of two κ-μ variates has also been addressed in [27]. However, the solutions in both works drastically differ from each other in several aspects. The approach taken here makes use of the sum of gamma variates, whereas in [27] the inverse Melin transform is used. The final expressions in both, obviously leading to the same numerical results, are given in very different functional forms. In addition, whereas in [27] the difference of the μ parameters cannot be an integer number (although the limit exists and can be determined), here no such restriction exists. Furthermore, several different applications are exercised in the present paper, including two involving field measurements.

The remainder of this paper is organized as follows. Section II presents the definition of the κ-μ fading model whilst Section III discusses the product distribution and provides the statistical characteristics of the double κ-μ fading model. Section IV discuss some performance measures whilst Section V presents some special cases and numerical results. Section VI presents some applications of the formulations presented in this paper and lastly, Section VII finishes the paper with some concluding remarks.

II. Definition

Let us consider two independent κ-μ distributed RVs, each with PDF

$$f_{R_i}(r) = \frac{2\mu_i (1+\kappa_i)^{\frac{\mu_i+1}{2}} r^{\mu_i}}{\kappa_i^{\frac{\mu_i-1}{2}} \mathrm{e}^{\mu_i \kappa_i} \hat{r}_i^{\mu_i+1}} \mathrm{e}^{\frac{-\mu_i(1+\kappa_i)r^2}{\hat{r}_i^2}} \times \mathrm{I}_{\mu_i-1}\left(2\mu_i \sqrt{\kappa_i (1+\kappa_i)} \frac{r}{\hat{r}_i}\right) \quad (1)$$

where $i = 1, 2$; $\kappa_i > 0$ is the ratio of the total power of the dominant components to the total power of the scattered waves, $\mu_i > 0$ is related to the number of multipath clusters, $\mathrm{I}_\nu(\cdot)$ is the modified Bessel function of the first kind and order ν [28, 8.406] and $\hat{r}_i$ is the root-mean square (rms) value of the received signal envelope, R_i. From [18],

$$\hat{r}_i \triangleq \sqrt{\mathbb{E}[R_i^2]} = \frac{\bar{r}_i \Gamma(\mu_i) [(1+\kappa_i)\mu_i]^{\frac{1}{2}}}{\Gamma\left(\mu_i + \frac{1}{2}\right) \mathrm{e}^{-\kappa_i \mu_i} {}_1F_1\left(\mu_i + \frac{1}{2}; \mu_i; \kappa_i \mu_i\right)}, \quad (2)$$

$$\mathbb{E}[R_i^k] = \frac{\hat{r}_i^k \Gamma\left(\mu_i + \frac{k}{2}\right) \mathrm{e}^{-\kappa_i \mu_i}}{\Gamma(\mu_i) [(1+\kappa_i)\mu_i]^{\frac{k}{2}}} {}_1F_1\left(\mu_i + \frac{k}{2}; \mu_i; \kappa_i \mu_i\right) \quad (3)$$

where $\bar{r}_i = \mathbb{E}[R_i]$, with $\mathbb{E}[\cdot]$ denoting the expectation operator, $\mathbb{E}[R_i^k]$ represents the kth moment of R_i, $\Gamma(\cdot)$ is the

TABLE I
COMMON PARAMETERS

Parameter	Description
i	Subindex for defining the i^{th}RV. Here $i = \{1, 2\}$
R_i	Received signal envelope
κ_i	Ratio between the total power of the dominant components and the scattered waves
μ_i	Real-valued extension related to the number of multipath clusters
$\hat{r_i}$	Root-mean square value of the received signal envelope
$\bar{r_i}$	Mean value of the received signal envelope
γ_i	Instantaneous signal-to-noise ratio
$\bar{\gamma_i}$	Average signal-to-noise ratio
K_i	Rician K factor defined as the ratio of the power of the dominant component and the scattered waves
m_i	Shaping parameter of a Nakagami-m RV
β_i	Shaping parameter of a Gamma RV
λ_i	Rate parameter (or inverse scale parameter) of a Gamma RV
m, n, j	Summation index
P, Q	Summation index

gamma function and ${}_1F_1\,(a; b; z)$ denotes the confluent hypergeometric function [28, 9.210.1].

Now, letting γ_i represent the instantaneous signal-to-noise-ratio (SNR) of a κ-μ fading channel, the PDF of its instantaneous SNR, $f_{\gamma_i}(\gamma)$, can be obtained from the envelope PDF given in (1) via a transformation of variables $\left(r = \sqrt{\gamma\ \hat{r}_i^2/\bar{\gamma}_i}\right)$ as

$$f_{\gamma_i}(\gamma) = \frac{\mu_i(1+\kappa_i)^{\frac{\mu_i+1}{2}}\gamma^{\frac{\mu_i-1}{2}}}{\kappa_i^{\frac{\mu_i-1}{2}}\mathrm{e}^{\mu_i\kappa_i}\bar{\gamma}_i^{\frac{\mu_i+1}{2}}}\mathrm{e}^{\frac{-\mu_i(1+\kappa_i)\gamma}{\bar{\gamma}_i}} \times \mathrm{I}_{\mu_i-1}\left(2\mu_i\sqrt{\frac{\kappa_i\,(1+\kappa_i)\,\gamma}{\bar{\gamma}_i}}\right) \quad (4)$$

where $\bar{\gamma}_i = \mathbb{E}[\gamma_i]$. Substituting for the modified Bessel function of the first kind from [29, eq. 9.6.16] as $\mathrm{I}_\nu(p) = \sum_{a'=0}^{\infty}\frac{1}{a'!\,\Gamma(a'+\nu+1)}\left(\frac{p}{2}\right)^{2a'+\nu}$ and defining $\theta_i = \frac{\mu_i(1+\kappa_i)}{\bar{\gamma}_i}$, (4) can be re-written as

$$\begin{aligned} f_{\gamma_i}(\gamma) &= \frac{1}{\mathrm{e}^{\mu_i\kappa_i}}\sum_{a'=0}^{\infty}\frac{(\mu_i\kappa_i)^{a'}}{a'!} \times\left[\frac{\theta_i^{a'+\mu_i}}{\Gamma(a'+\mu_i)}\gamma^{a'+\mu_i-1}\exp(-\gamma\,\theta_i)\right] \\ &= \frac{1}{\mathrm{e}^{\mu_i\kappa_i}}\sum_{a'=0}^{\infty}\frac{(\mu_i\kappa_i)^{a'}}{a'!}gamma\left(a'+\mu_i, \theta_i\right), \end{aligned} \quad (5)$$

where $a' = m, n$; $i = 1, 2$ and $gamma(\beta_i, \lambda_i)$ denotes the PDF of the gamma distribution shown in (6).

$$f_{\acute{Z}_i}\left(\acute{z}\right) = \frac{\lambda_i^{\beta_i}}{\Gamma\left(\beta_i\right)}\acute{z}^{\beta_i-1}e^{-\acute{z}\lambda_i} \quad (6)$$

where β_i denotes the shape parameter and λ_i denotes the rate parameter (i.e, an inverse scale parameter). The notations used in this paper are summarized in Table I.

III. FORMULATIONS

Following a similar approach to the one presented in [15] and [30], in this section we derive the product distribution of $X = \gamma_1\gamma_2$, of the double κ-μ faded channel.

A. PDF and CDF of the Double κ-μ Fading Model

Since the PDF of γ_1 and γ_2 are linear combinations of the gamma distribution, the PDF of the product term, $X = \gamma_1\gamma_2$, can be readily evaluated from [30, Lemma 2] as follows

$$f_X(x) = \frac{\theta_1\theta_2}{\rho_{1,2}}\sum_{m=0}^{\infty}\sum_{n=0}^{\infty}c_{n,m}G_{0,2}^{2,0}(x\theta_1\theta_2|_{m+\mu_1-1,\ n+\mu_2-1}) \quad (7)$$

where $G_{p'q'}^{m'n'}(z\,|\ldots)$ is the Meijer G-function,[1] $\rho_{1,2} = \mathrm{e}^{\mu_1\kappa_1+\mu_2\kappa_2}$ and $c_{n,m} \triangleq \frac{(\kappa_1\mu_1)^m(\kappa_2\mu_2)^n}{m!n!\Gamma(m+\mu_1)\Gamma(n+\mu_2)}$. Now, substituting $Y^2 = X$ followed by a transformation of variable in (7), we obtain the envelope PDF of the product term, $Y = R_1R_2$, as follows

$$f_Y(y) = \frac{2y\phi_1\phi_2}{\rho_{1,2}}\sum_{m=0}^{\infty}\sum_{n=0}^{\infty}c_{n,m}G_{0,2}^{2,0}\left(y^2\phi_1\phi_2\Big|_{m+\mu_1-1,\ n+\mu_2-1}\right) \quad (8)$$

[1]The Meijer G-function is now a standard built-in function in well-known mathematical software packages, such as Mathematica and Matlab. As well as this, it can be expressed in terms of the more familiar generalized hypergeometric functions [31]. Nonetheless, where possible, in this work we provide alternative expressions in non-Meijer G form.

$$f_X(x) = \frac{2}{x\rho_{1,2}}\Bigg[\sum_{j=1}^{\infty}\left(\frac{x}{\mathcal{K}_1\mathcal{K}_2}\right)^{\frac{\xi_3}{2}}(\kappa_1\mu_1)^j\,\mathrm{K}_{j+\mu_1-\mu_2}\left(2\sqrt{\frac{x}{\mathcal{K}_1\mathcal{K}_2}}\right){}_0\widetilde{F}_3\left(;1+j,j+\mu_1,\mu_2;\zeta_1\right) + \sum_{j=0}^{\infty}\left(\frac{x}{\mathcal{K}_1\mathcal{K}_2}\right)^{\frac{\xi_3}{2}}(\kappa_2\mu_2)^j\,\mathrm{K}_{j-\mu_1+\mu_2}\left(2\sqrt{\frac{x}{\mathcal{K}_1\mathcal{K}_2}}\right){}_0\widetilde{F}_3\left(;1+j,\mu_1,j+\mu_2;\zeta_1\right)\Bigg]. \tag{9}$$

$$f_Y(y) = \frac{4}{y\rho_{1,2}}\Bigg[\sum_{j=1}^{\infty}\left(\frac{y^2}{\mathcal{P}_1\mathcal{P}_2}\right)^{\frac{\xi_3}{2}}(\kappa_1\mu_1)^j\,\mathrm{K}_{j+\mu_1-\mu_2}\left(2y\sqrt{\frac{1}{\mathcal{P}_1\mathcal{P}_2}}\right){}_0\widetilde{F}_3\left(;1+j,j+\mu_1,\mu_2;\zeta_2\right) + \sum_{j=0}^{\infty}\left(\frac{y^2}{\mathcal{P}_1\mathcal{P}_2}\right)^{\frac{\xi_3}{2}}(\kappa_2\mu_2)^j\,\mathrm{K}_{j-\mu_1+\mu_2}\left(2y\sqrt{\frac{1}{\mathcal{P}_1\mathcal{P}_2}}\right){}_0\widetilde{F}_3\left(;1+j,\mu_1,j+\mu_2;\zeta_2\right)\Bigg]. \tag{10}$$

where $\phi_i = \frac{\mu_i(1+\kappa_i)}{\hat{r}_i^{\,2}}$, $\rho_{1,2}$ and $c_{n,m}$ are as defined previously.

Performing some mathematical manipulations on (7), the PDF of the product distribution simplifies to (9), as shown at the top of this page. Here, $\mathcal{K}_1 = 1/\theta_1$, $\mathcal{K}_2 = 1/\theta_2$, $\zeta_1 = \frac{x\kappa_1\kappa_2\mu_1\mu_2}{\mathcal{K}_1\mathcal{K}_2}$, $\xi_3 = j+\mu_1+\mu_2$, $\mathrm{K}_\phi(\cdot)$ is the ϕth-order modified Bessel function of the second kind [28, 8.432] and ${}_p\widetilde{F}_q\left(\{a_1,a_2\cdots a_q\};\{b_1,b_2\cdots b_q\};z\right)$ is the regularized Hypergeometric function [32]. The proof of (9) is shown in Appendix A. Of course, substituting $Y^2 = X$ followed by a transformation of variable in (9), we obtain the envelope PDF of the product term, as shown in (10) at the top of this page. Here, $\mathcal{P}_1 = 1/\phi_1$, $\mathcal{P}_2 = 1/\phi_2$, $\xi_3 = j+\mu_1+\mu_2$ and $\zeta_2 = \frac{y^2\kappa_1\kappa_2\mu_1\mu_2}{\mathcal{P}_1\mathcal{P}_2}$.

In a similar manner, the CDF of the product of two κ-μ RVs can be obtained from [30, Lemma 2] as

$$F_X(x) = \frac{1}{\rho_{1,2}}\sum_{m=0}^{\infty}\sum_{n=0}^{\infty}c_{n,m}G_{1,3}^{2,1}\left(x\theta_1\theta_2\middle|\begin{matrix}\ \\ m+\mu_1,\ n+\mu_2,\ 0\end{matrix}\right), \tag{11}$$

where $\rho_{1,2}$ and $c_{n,m}$ are as defined previously. The CDF of its signal envelope Y is given by

$$F_Y(y) = F_X(y^2) = \frac{1}{\rho_{1,2}}\sum_{m=0}^{\infty}\sum_{n=0}^{\infty}c_{n,m}G_{1,3}^{2,1}\left(y^2\phi_1\phi_2\middle|\begin{matrix}\ \\ m+\mu_1,\ n+\mu_2,\ 0\end{matrix}\right). \tag{12}$$

In the following, we derive analytical and closed-form expressions for the MGF and higher order moments of the product distribution, $X = \gamma_1\gamma_2$ using (7) and (9).

B. Moment Generating Function

The moment generating function of the product distribution, $X = \gamma_1\gamma_2$, is given by

$$M_X(-s) \triangleq \mathbb{E}\left[\mathrm{e}^{-\mathrm{s}X}\right] = \int_0^\infty \mathrm{e}^{-sx}f_X(x)\,dx. \tag{13}$$

Substituting (7) in (13), followed by the mathematical manipulations shown in Appendix B, we obtain the MGF of the double κ-μ fading channel as

$$\mathbb{E}\left[\mathrm{e}^{sX}\right] = \frac{1}{\rho_{1,2}}\sum_{m=0}^{\infty}\sum_{n=0}^{\infty}c_{n,m}G_{2,1}^{1,2}\left(\frac{s}{\theta_1\theta_2}\middle|\begin{matrix}1-m-\mu_1,\ 1-n-\mu_2\\ 0\end{matrix}\right) = \sum_{m=0}^{\infty}\sum_{n=0}^{\infty}\frac{(\kappa_1\mu_1)^m(\kappa_2\mu_2)^n}{\rho_{1,2}m!n!}\left(\frac{\theta_1\theta_2}{s}\right)^{m+\mu_1} \times\mathrm{U}\left(m+\mu_1,1-n+m+\mu_1-\mu_2,\frac{\theta_1\theta_2}{s}\right) \tag{14}$$

where $\rho_{1,2}$ and $c_{n,m}$ are as defined previously, and $\mathrm{U}(\cdot,\cdot,\cdot)$ is the confluent Tricomi hypergeometric function [29, eq. 13.1.3].

C. Higher Order Moments

The q-th order moment of the product distribution is defined as $\mathbb{E}\left[X^q\right] \triangleq \int_0^\infty x^q f_X(x)\,dx$. It is worth remarking that since we consider two statistically independent κ-μ distributed RVs, the q-th order moment of the product distribution is the product of the individual moments i.e., $\mathbb{E}\left[X^q\right] = \mathbb{E}\left[\gamma_1^q\right]\mathbb{E}\left[\gamma_2^q\right]$. Using the relationship $\mathbb{E}\left[R_i^q\right] = \mathbb{E}\left[\gamma_i^{\frac{q}{2}}\right]$ and substituting for $\mathbb{E}\left[R_i^q\right]$ from (3), we obtain

$$\mathbb{E}\left[X^q\right] = \frac{(\mu_1)_q\,(\mu_2)_q}{\rho_{1,2}\,\theta_1^q\theta_2^q} \times{}_1F_1(q+\mu_1;\mu_1;\kappa_1\mu_1)\,{}_1F_1(q+\mu_2;\mu_2;\kappa_2\mu_2) \tag{15}$$

where $\rho_{1,2}$ is as defined previously and $(\tau_1)_{\tau_2} = \frac{\Gamma(\tau_1+\tau_2)}{\Gamma(\tau_1)}$ is the Pochhammer symbol.

D. κ-μ/κ-μ Composite Fading Statistics

To obtain the κ-μ/κ-μ composite fading statistics we consider that the small-scale fading is described by a κ-μ RV with parameters $\{\kappa_1,\ \mu_1,\ \bar{r}_1\}$. Additionally, we assume that the mean of this RV follows another κ-μ distribution, with parameters $\{\kappa_2,\ \mu_2,\ \bar{r}_2\}$, that describes the shadowing. It is noteworthy that the composite fading statistics can be found as a particular case of the statistics of the product of RVs. According to [16], the composite fading statistics can be obtained from the product of two RVs by assuming that the mean value of one of the RVs is equal to one. Therefore,

the envelope PDF and CDF of the κ-μ/κ-μ composite fading model can be obtained by first setting $\bar{r}_1 = 1$ in (2) and then substituting the resultant $\hat{r}_1$ in (10) and (12), respectively.

IV. Performance Analysis and Approximate Expressions

In this section, we derive closed-form expressions for the amount of fading and channel quality estimation index, whilst analytical formulations are obtained for the outage probability, average channel capacity, average symbol error probability and average bit error probability of the double κ-μ fading channel. Additionally, we obtain approximate closed-form expressions for the PDF, CDF and MGF of the product of two κ-μ RVs.

A. Amount of Fading

The amount of fading is often used to quantify the severity of fading experienced during transmission over fading channels. It is defined by [17, eq. 1] as

$$\mathrm{AF} \triangleq \frac{\mathbb{V}[X]}{\mathbb{E}[X]^2} = \frac{\mathbb{E}\left[X^2\right] - \mathbb{E}[X]^2}{\mathbb{E}[X]^2} = \frac{\mathbb{E}\left[X^2\right]}{\mathbb{E}[X]^2} - 1 \quad (16)$$

where $\mathbb{V}[\cdot]$ denotes the variance operator. Substituting for $\mathbb{E}[X]$ and $\mathbb{E}\left[X^2\right]$ from (15), followed by some algebraic manipulations a closed-form expression for the AF of the product distribution is obtained as

$$\mathrm{AF} = \left(1 + \frac{2\kappa_1 + 1}{\mu_1(1+\kappa_1)^2}\right)\left(1 + \frac{2\kappa_2 + 1}{\mu_2(1+\kappa_2)^2}\right) - 1. \quad (17)$$

The proof of (17) can be found in Appendix C.

B. Channel Quality Estimation Index

For a given fading distribution, the channel quality estimation index is defined as the ratio of the variance of the instantaneous received SNR to the cubed mean of the received SNR and is directly related to the system's average error rate [33] i.e,

$$\mathrm{CQEI} = \frac{\mathbb{V}[X]}{[\mathbb{E}(X)]^3} = \frac{\mathrm{AF}}{\mathbb{E}[X]}. \quad (18)$$

Substituting for AF and $\mathbb{E}[X]$ from (17) and (36) respectively, a closed-form expression for the CQEI of the product distribution can be obtained as follows

$$\mathrm{CQEI} = \frac{1}{\bar{\gamma}_1\bar{\gamma}_2}\left[\left(1 + \frac{2\kappa_1+1}{\mu_1(1+\kappa_1)^2}\right)\left(1 + \frac{2\kappa_2+1}{\mu_2(1+\kappa_2)^2}\right) - 1\right]. \quad (19)$$

C. Outage Probability

The outage probability of a communication system is defined as the probability that the instantaneous SNR drops below a given threshold, γ_{th}. Using (11), this probability can be obtained as

$$P_{\mathrm{OP}}(\gamma_{\mathrm{th}}) = \frac{1}{\rho_{1,2}} \sum_{m=0}^{\infty}\sum_{n=0}^{\infty} c_{n,m} G_{1,3}^{2,1}\left(\gamma_{\mathrm{th}}\theta_1\theta_2 \middle|\, {}_{m+\mu_1,\ n+\mu_2,\ 0}^{\ 1}\right) \quad (20)$$

where $\rho_{1,2}$ and $c_{n,m}$ are as defined previously.

D. Average Channel Capacity

The bandwidth normalized average channel capacity (ACC) is defined as [34]

$$\frac{C}{W} \triangleq \int_0^{\infty} \log_2(1+x)\, f_X(x)\, dx \quad (21)$$

where W is the fading channel bandwidth, C its ACC and $f_X(\cdot)$ denotes the PDF. Substituting (7) in (21), followed by the mathematical manipulations shown in Appendix D, we obtain the ACC of the double κ-μ fading channel as

$$\frac{C}{W} = \frac{1}{\rho_{1,2}} \sum_{m=0}^{\infty}\sum_{n=0}^{\infty} c_{n,m} G_{2,4}^{4,1}\left(\theta_1\theta_2 \middle|\, {}_{-1,\ m+\mu_1-1,\ n+\mu_2-1}^{-1,\ 0}\right) \quad (22)$$

where $\rho_{1,2}$ and $c_{n,m}$ are as defined previously.

E. Average Symbol and Bit Error Probability

The MGF can be used to evaluate the average symbol error probability (SEP) and average bit error probability (BEP) for several different modulation schemes. For example, the MGF based average BEP for a differential phase shift keying (DPSK) modulation scheme can be expressed as [35, eq. 6.70]

$$\bar{P}_b = c_1 M_X(-c_2) \quad (23)$$

where $M_X(\cdot)$ denotes the MGF, c_1 and c_2 represent constants that depend on the chosen modulation scheme. For the DPSK modulation scheme, $c_1 = 0.5$ and $c_2 = 1$ [35].

The average SEP of a communication system for an M-ary phase shift keying (MPSK) modulation scheme can be expressed as [35, eq. 6.75]

$$\bar{P}_s = \frac{1}{\pi}\int_0^{\frac{(\mathrm{M}-1)\pi}{\mathrm{M}}} M_X\left(-\frac{g}{\mathrm{Sin}^2\phi}\right) d\phi \quad (24)$$

where $M_X(\cdot)$ denotes the MGF and $g = \mathrm{Sin}^2(\pi/\mathrm{M})$ depends on the size of the MPSK constellation. For example, $\mathrm{M} = 2$ for a BPSK modulation scheme, and $\mathrm{M} = 4$ for a QPSK modulation scheme. Thus, the average BEP and SEP for the double κ-μ fading channel can be obtained by substituting (14) in (23) and (24), respectively.

F. Approximate Closed-Form Expressions

The series representation of the modified Bessel function of the first kind used in this study, although relatively simple, has an infinite form which raises the need for approximate asymptotic solutions [36]. To this end, [36] derives a useful approximation for $\mathrm{I}_v(p)$ which retains high accuracy and simple algebraic form of the original series representation. The approximate series form is given by [36, eq. 19]

$$\mathrm{I}_v(p) \simeq \sum_{a'=0}^{b'} \frac{\Gamma\left(b'+a'\right)}{\Gamma(a'+1)\,\Gamma(b'-a'+1)\,\Gamma(a'+v+1)}\left(\frac{p}{2}\right)^{2a'+v} \quad (25)$$

and is valid for $0 < p < 2b'$. When $b' \to \infty$, the above expression is equivalent to the original infinite series representation of $\mathrm{I}_v(p)$, [36].

TABLE II
SPECIAL CASES OF THE DOUBLE κ-μ FADING MODEL*

Fading model	Double κ-μ parameters	PDF expression for the special case
double Rayleigh [7]	$\underline{\kappa_1} \to 0$, $\underline{\mu_1} = 1$ $\underline{\kappa_2} \to 0$ $\underline{\mu_2} = 1$	$\frac{4y}{\hat{r}_1^2 \hat{r}_2^2} \mathrm{K}_0 \left(\frac{2y}{\hat{r}_1 \hat{r}_2} \right)$
double Rice [38]	$\underline{\kappa_1} = K_1$, $\underline{\mu_1} = 1$ $\underline{\kappa_2} = K_2$, $\underline{\mu_2} = 1$	$\sum_{m=0}^{\infty} \sum_{n=0}^{\infty} \frac{4y^{1+n+m} K_1^m K_2^n \left(\Delta_1 \Delta_2\right)^{\frac{1}{2}(2+n+m)}}{\mathrm{e}^{\mathrm{K}_1+\mathrm{K}_2} \left(n!\right)^2 \left(m!\right)^2} \mathrm{K}_{m-n} \left(2y \sqrt{\Delta_1 \Delta_2} \right)$
double Nakagami-m [15]	$\underline{\kappa_1} \to 0$, $\underline{\mu_1} = m_1$ $\underline{\kappa_2} \to 0$, $\underline{\mu_2} = m_2$	$\frac{4y^{m_1+m_2-1}}{\Gamma\left(m_1\right)\Gamma\left(m_2\right)} \left(\frac{m_1 m_2}{\hat{r}_1^2 \hat{r}_2^2} \right)^{\frac{m_1+m_2}{2}} \mathrm{K}_{m_1-m_2} \left(2y \sqrt{\frac{m_1 m_2}{\hat{r}_1^2 \hat{r}_2^2}} \right)$
double One-Sided Gaussian [15]	$\underline{\kappa_1} \to 0$, $\underline{\mu_1} = 0.5$, $\underline{\kappa_2} \to 0$, $\underline{\mu_2} = 0.5$	$\frac{2}{\Gamma\left(0.5\right)^2} \frac{1}{\hat{r}_1 \hat{r}_2} \mathrm{K}_0 \left(\frac{y}{\hat{r}_1 \hat{r}_2} \right)$
κ-μ / Rice	$\underline{\kappa_2} = K_2$, $\underline{\mu_2} = 1$	$\sum_{m=0}^{\infty} \sum_{n=0}^{\infty} \frac{4y^{n+m+\mu_1} \left(\kappa_1 \mu_1\right)^m K_2^n \left(\phi_1 \Delta_2\right)^{\frac{1}{2}(1+n+m+\mu_1)}}{\mathrm{e}^{\kappa_1 \mu_1 + \mathrm{K}_2} \left(n!\right)^2 m! \Gamma\left(\mu_1+m\right)} \mathrm{K}_{m-n+\mu_1-1} \left(2y \sqrt{\phi_1 \Delta_2} \right)$
κ-μ / Nakagami-m	$\underline{\kappa_2} \to 0$, $\underline{\mu_2} = m_2$	$\sum_{m=0}^{\infty} \frac{4y^{m+\mu_1+m_2-1} \left(\kappa_1 \mu_1\right)^m \left(\phi_1 m_2 / \hat{r}_2\right)^{\frac{1}{2}(m+\mu_1+m_2)}}{\mathrm{e}^{\kappa_1 \mu_1} m! \Gamma\left(\mu_1+m\right) \Gamma\left(m_2\right)} \mathrm{K}_{m+\mu_1-m_2} \left(2y \sqrt{\frac{\phi_1 m_2}{\hat{r}_2}} \right)$
κ-μ / Rayleigh	$\underline{\kappa_2} \to 0$, $\underline{\mu_2} = 1$	$\sum_{m=0}^{\infty} \frac{4y^{m+\mu_1} \left(\kappa_1 \mu_1\right)^m \left(\phi_1 / \hat{r}_2\right)^{\frac{1}{2}(m+\mu_1+1)}}{\mathrm{e}^{\kappa_1 \mu_1} m! \Gamma\left(\mu_1+m\right)} \mathrm{K}_{m+\mu_1-1} \left(2y \sqrt{\frac{\phi_1}{\hat{r}_2}} \right)$
Rayleigh / Nakagami-m	$\underline{\kappa_1} \to 0$, $\underline{\mu_1} = 1$ $\underline{\kappa_2} \to 0$, $\underline{\mu_2} = m_2$	$\frac{4y^{m_2}}{\Gamma\left(m_2\right)} \left(\frac{m_2}{\hat{r}_1^2 \hat{r}_2^2} \right)^{\frac{1+m_2}{2}} \mathrm{K}_{1-m_2} \left(2y \sqrt{\frac{m_2}{\hat{r}_1^2 \hat{r}_2^2}} \right)$
Rice / Nakagami-m	$\underline{\kappa_1} = K_1$, $\underline{\mu_1} = 1$ $\underline{\kappa_2} \to 0$, $\underline{\mu_2} = m_2$	$\sum_{m=0}^{\infty} \frac{4y^{m+m_2} K_1^m \left(\Delta_1 m_2 / \hat{r}_2\right)^{\frac{1}{2}(1+m+m_2)}}{\mathrm{e}^{\mathrm{K}_1} \left(m!\right)^2 \Gamma\left(m_2\right)} \mathrm{K}_{m-m_2+1} \left(2y \sqrt{\frac{\Delta_1 m_2}{\hat{r}_2}} \right)$
One-sided Gaussian / Nakagami-m	$\underline{\kappa_1} = 0$, $\underline{\mu_1} = 0.5$ $\underline{\kappa_2} \to 0$, $\underline{\mu_2} = m_2$	$\frac{4y^{m_2-0.5}}{\Gamma\left(0.5\right)\Gamma\left(m_2\right)} \left(\frac{0.5 m_2}{\hat{r}_1^2 \hat{r}_2^2} \right)^{\frac{0.5+m_2}{2}} \mathrm{K}_{0.5-m_2} \left(2y \sqrt{\frac{0.5 m_2}{\hat{r}_1^2 \hat{r}_2^2}} \right)$

*Where necessary approximate closed-form expressions can be obtained by first substituting [39, 07.34.03.0605.01] in the approximate PDF expression (see (26)), followed by appropriate substitutions for the κ_i and μ_i parameters.

Now, substituting (25) in (4) and following a similar mathematical approach to that given in Section III.A and B, approximate closed-form expressions for the PDF, CDF and MGF of the double κ-μ distribution are obtained as

$$f_X(x) = \frac{\theta_1 \theta_2}{\rho_{1,2}} \sum_{m=0}^{P} \sum_{n=0}^{Q} \mathcal{G} c_{n,m} \times G_{0,2}^{2,0} \left(x\ \theta_1 \theta_2 \middle|\ {}_{m+\mu_1-1,\ n+\mu_2-1} \right), \tag{26}$$

$$F_X(x) = \frac{1}{\rho_{1,2}} \sum_{m=0}^{P} \sum_{n=0}^{Q} \mathcal{G} c_{n,m} \times G_{1,3}^{2,1} \left(x\ \theta_1 \theta_2 \middle|\ {}_{m+\mu_1,\ n+\mu_2,\ 0}^{1} \right), \tag{27}$$

$$\mathbb{E}\left[\mathrm{e}^{sX} \right] = \sum_{m=0}^{P} \sum_{n=0}^{Q} \mathcal{G} \frac{\left(\kappa_1 \mu_1\right)^m \left(\kappa_2 \mu_2\right)^n}{\rho_{1,2} m! n!} \left(\frac{\theta_1 \theta_2}{s} \right)^{m+\mu_1} \times \mathrm{U} \left(m+\mu_1, 1-n+m+\mu_1-\mu_2, \frac{\theta_1 \theta_2}{s} \right). \tag{28}$$

Here, $\mathcal{G} = \frac{\Gamma(m+P)\Gamma(n+Q) P^{1-2m} Q^{1-2n}}{\Gamma(P-m+1)\Gamma(Q-n+1)}$, $c_{n,m}$ and $\rho_{1,2}$ are as defined before.

V. SPECIAL CASES AND NUMERICAL RESULTS

A. Some Special Cases

The PDFs given in (7) and (8) represent an extremely versatile set of fading conditions as they contain the double Rayleigh, double Rician, double Nakagami-m and double One-Sided Gaussian fading models as special cases. For instance, using [38, 07.34.03.0605.01], and substituting $\kappa_i = K_i$ and $\mu_i = 1$ in (8), we obtain the PDF of the product of two Rician RVs, such as that presented in [37].

Of course, allowing $\kappa_i \to 0$ and $\mu_i = 1$, we obtain the PDF of the double Rayleigh fading model [7]. Now substituting [38, 07.34.03.0605.01], $\kappa_i \to 0$ and $\mu_i = m_i$ in (8) we obtain the PDF of the product of two Nakagami-m RVs, equivalent to the result presented in [15, eq. 6]. It is worth highlighting that the double Rayleigh and double Nakagami-m fading models were used to characterize keyhole channels in MIMO systems in [9] and [10], respectively. Furthermore, the product of Nakagami-m RVs, and One-Sided Gaussian RVs were used to study the performance metrics of cascaded fading channels in [15] and [16], respectively. The product distribution also

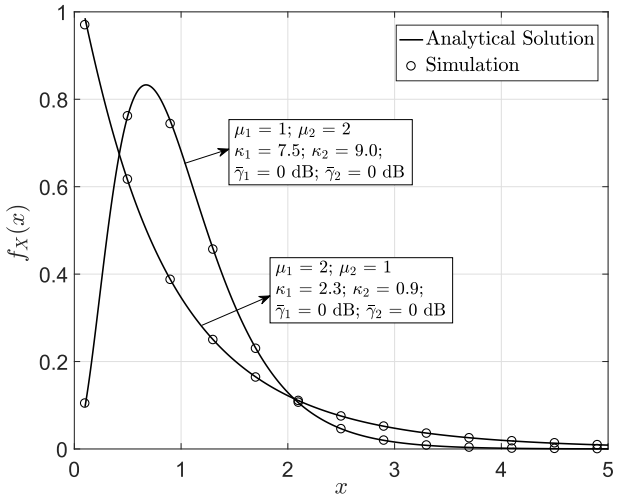

Fig. 1. The PDF of the product of two κ-μ RVs. $\{\mu_1, \mu_2\} = \{1,2\}, \{2,1\}$; $\{\kappa_1, \kappa_2\} = \{7.5,9.0\}, \{2.3,0.9\}$ and $\bar{\gamma}_1 = \bar{\gamma}_2 = 0$ dB. Lines represent the analytical results and circle markers represent simulation results.

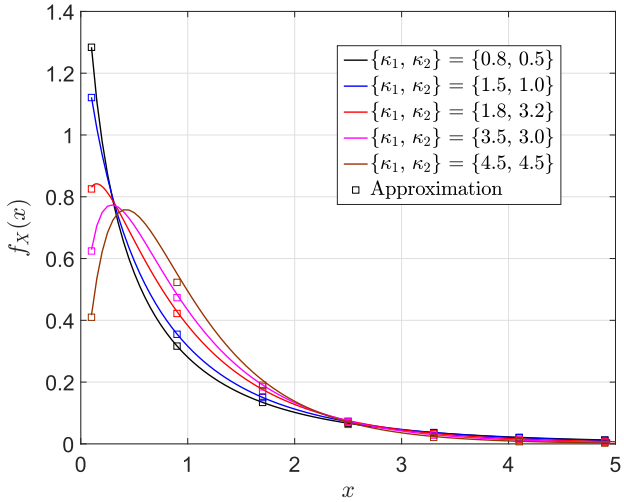

Fig. 2. The PDF of the product of two κ-μ RVs for a wide range of $\{\kappa_1, \kappa_2\}$, with $\{\mu_1, \mu_2\} = \{1.1,1.3\}$ and $\bar{\gamma}_1 = \bar{\gamma}_2 = 0$ dB. Lines represent the analytical results and square markers represents the approximate closed-form expression.

finds application in the computation of the composite fading statistics which is obtained as a particular case of the product of two RVs (see Section III-D).

The double κ-μ PDF also encompasses product mixtures of the Rayleigh, Rice, Nakagami-m and One-Sided Gaussian RVs as special cases. For example, the PDFs of the product of κ-μ/Rice, κ-μ/Rayleigh, Rayleigh/Nakagami-m, One-sided Gaussian/Nakagami-m can be obtained from (8) by first using [38, 07.34.03.0605.01], followed by appropriate substitutions for the κ_i and μ_i parameters. Table II summarizes some special cases of the double κ-μ distribution along with their PDFs, where $\Delta_1 = \frac{K_1+1}{\hat{r}_1^2}$ and $\Delta_2 = \frac{K_2+1}{\hat{r}_2^2}$. For the sake of clarity, the double κ-μ parameters have been underlined and where possible, closed-form expressions for the special case results have been deduced.

B. Numerical Results

Plots for the PDF of the double κ-μ distribution for different values of κ, μ and $\bar{\gamma}$ are shown in Figs. 1, 2 and 3. Over the three figures, the values of the parameters are chosen to illustrate the wide range of shapes that the product distribution can exhibit. Fig. 1 shows the PDF of the double κ-μ distribution for two sets of $\{\mu_1, \mu_2\}$ i.e, $\{\mu_1, \mu_2\} = \{1, 2\}, \{2, 1\}$, with $\{\kappa_1, \kappa_2\} = \{7.5, 9.0\}, \{2.3, 0.9\}$ and $\bar{\gamma}_1 = \bar{\gamma}_2 = 0$ dB. The number of terms in the series required for a given accuracy varies with the parameters. However, for the PDF plots shown here, P and Q were chosen to be 50. Furthermore, in all cases, the analytical results agree with the Monte-Carlo simulations. Fig. 2 shows the PDF of the double κ-μ distribution for a wide range of $\{\kappa_1, \kappa_2\}$, with $\{\mu_1, \mu_2\} = \{1.1, 1.3\}$ and $\bar{\gamma}_1 = \bar{\gamma}_2 = 0$ dB. It can be seen that the approximate closed-form expression agrees well with the analytical results. From all three figures, we observe that lower values of the κ and μ parameters shift the curves closer to the y-axis whilst higher values shift the curves closer to $\bar{\gamma}_1\bar{\gamma}_2$ or $\bar{r}_1\bar{r}_2$. Fig 4 shows the double κ-μ CDF for a wide range of $\{\kappa_1, \kappa_2\}$, with $\{\mu_1, \mu_2\} = \{1.1, 1.3\}$ and $\bar{\gamma}_1 = \bar{\gamma}_2 = 0$ dB. A maximum of 100 terms

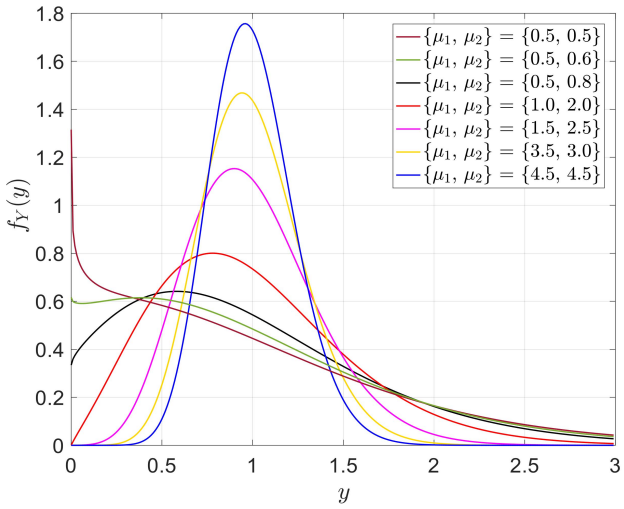

Fig. 3. κ-μ/κ-μ composite fading PDF for a wide range of $\{\mu_1, \mu_2\}$, with $\{\kappa_1, \kappa_2\} = \{4.1,2.0\}$ and $\bar{r}_2 = 1$.

were used (i.e, $P = Q = 100$) to implement the approximate CDF expression. There exists a difference in the number of terms chosen for the approximate PDF and CDF expressions due to the different Meijer-G term found in (27). Again, it can be seen that the approximate expression agrees well with the analytical results.

Fig. 5 illustrates the effect of the AF experienced in double κ-μ fading channels for a range of κ_1, κ_2, μ_1 and μ_2. It can clearly be seen that the greatest AF occurs for low values of the κ and μ parameters indicating that the channel is subject to severe multipath fading. On the other hand the value of the AF approaches 0 as the κ_1, κ_2, μ_1 and μ_2 parameters become large. Moreover, the case when the AF experienced by double κ-μ model coincides with the AF of the double Rician model is also indicated in Fig. 5. Depending on the μ_1 and μ_2 parameters, the AF experienced in double κ-μ fading channels can be greater or lower than that experienced in double Rician fading channels.

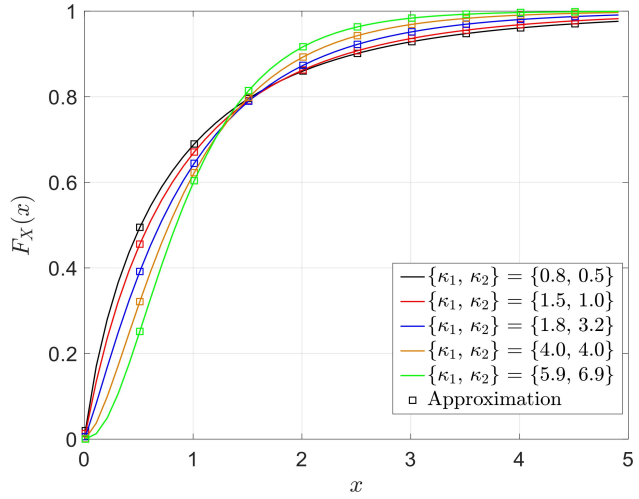

Fig. 4. The CDF of the product of two κ-μ RVs for a wide range of $\{\kappa_1, \kappa_2\}$, with $\{\mu_1, \mu_2\} = \{1.1,1.3\}$ and $\bar{\gamma}_1 = \bar{\gamma}_2 = 0$ dB. Lines represent the analytical results and square markers represent the approximate closed-form expression.

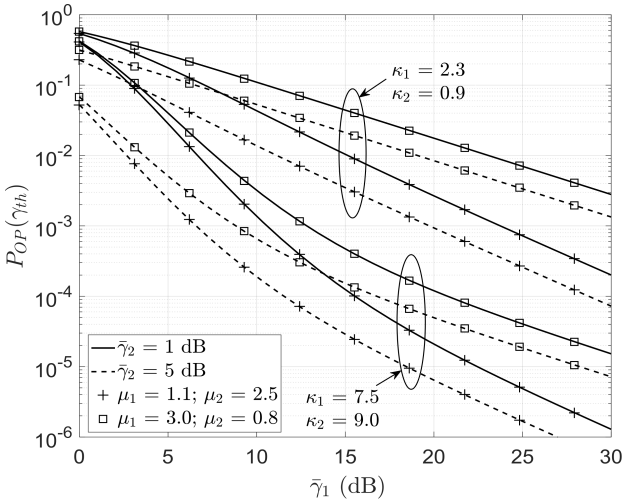

Fig. 6. Outage probability versus $\bar{\gamma}_1$ for different values of $\kappa_1, \kappa_2, \mu_1$ and μ_2. Here, $\gamma_{\text{th}} = 0$ dB and $\bar{\gamma}_2 = 1, 5$ dB.

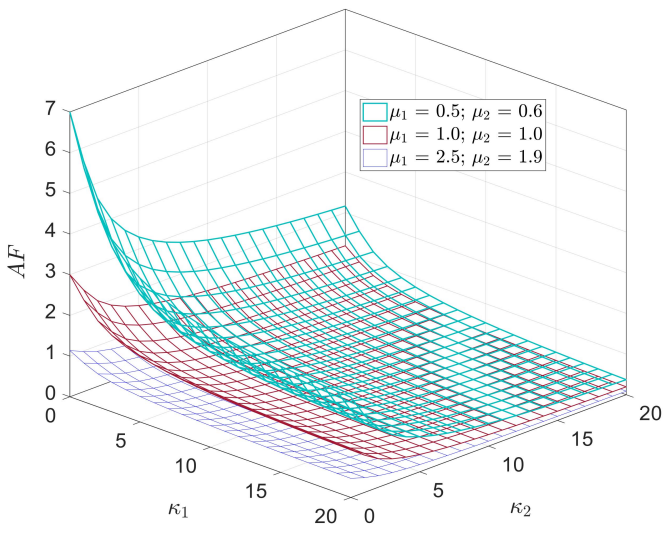

Fig. 5. The AF in double κ-μ fading channels for a range of κ_1 and κ_2 when $\{\mu_1, \mu_2\} = \{0.5, 0.6\}$ and $\{2.5, 1.9\}$. The AF of the double Rician fading model where $\{\mu_1, \mu_2\} = \{1\ 1\}$, is shown as a special case and is indicated by the burgundy lined mesh.

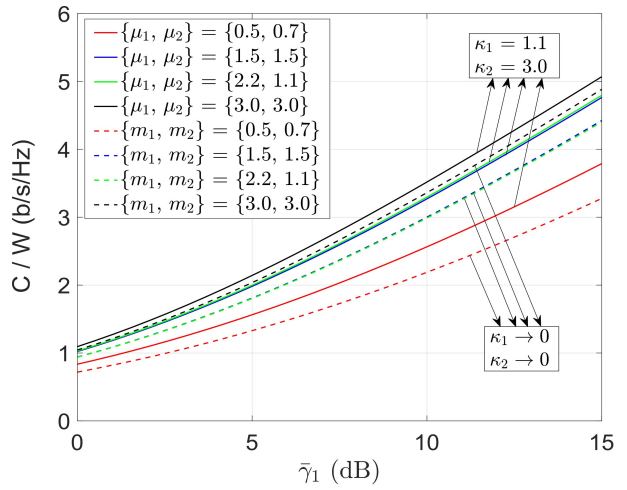

Fig. 7. ACC versus $\bar{\gamma}_1$ of the double κ-μ fading channel compared with the ACC of the double Nakagami-m fading model. Here, $\bar{\gamma}_2 = 1$ dB. Continuous lines represent the ACC of the double κ-μ fading model whilst dashed lines represent the ACC of the double Nakagami-m fading model.

Fig. 6 depicts the OP versus $\bar{\gamma}_1$ when $\gamma_{\text{th}} = 0$ dB, and for two sets of $\{\mu_1, \mu_2\}$ and $\{\kappa_1, \kappa_2\}$ i.e, $\{\mu_1, \mu_2\} = \{1.1, 2.5\}$, $\{3.0, 0.8\}$; $\{\kappa_1, \kappa_2\} = \{2.3, 0.9\}$, $\{7.5, 9.0\}$, with $\bar{\gamma}_2 = 1$ and 5 dB. We observe that the rate at which the outage probability decreases depends on the κ and μ parameters. For instance, the rate at which the outage probability decreases is slower when $\{\kappa_1, \kappa_2\} = \{2.3, 0.9\}$ compared to $\{\kappa_1, \kappa_2\} = \{7.5, 9.0\}$.

Fig. 7 shows the ACC of a double κ-μ fading channel as a function of $\bar{\gamma}_1$ for a range of $\{\mu_1, \mu_2\}$ when$\{\kappa_1, \kappa_2\} = \{1.1, 3.0\}$. Note that as μ_1 and μ_2 increase, the system capacity also increases. Similar performance improvement is observed as κ_1 and κ_2 increase. The figure also shows the ACC of a double Nakagami-m fading channel as a function of $\bar{\gamma}_1$ for a range of $\{m_1, m_2\}$ when $\bar{\gamma}_2 = 1$ dB. It can be seen that the ACC of the double κ-μ fading channel is higher compared to the ACC of the double Nakagami-m fading channel.

Figs. 8 and 9 depict the average BEP versus $\bar{\gamma}_1$ for a DPSK modulation scheme, and the average SEP versus $\bar{\gamma}_1$ for a BPSK modulation scheme when $\{\kappa_1, \kappa_2\} = \{1.5, 0.9\}$ and for different values of μ_1 and μ_2. The square markers in Fig. 8 represent the average BEP obtained using the approximate MGF expression. For the approximate closed-form expression, P and Q were chosen to be 50. We observe that the average BEP and the average SEP increase for lower values of μ_1 and μ_2, indicating that the system's performance will be degraded in environments that undergo a greater fading severity. Moreover, the rate at which the average BEP and the average SEP decrease is dominated by the μ parameters. For instance, the average BEP for $\{\mu_1, \mu_2\} = \{2.5, 3.2\}$ is lower compared to $\{\mu_1, \mu_2\} = \{0.5, 0.7\}$.

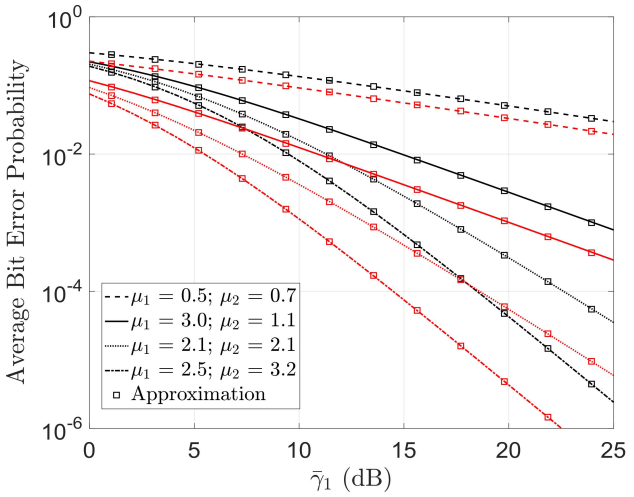

Fig. 8. Average BEP versus $\bar{\gamma}_1$ for a DPSK modulation scheme and for different values of μ_1 and μ_2. Here, $\bar{\gamma}_2 = 1, 5$ dB, and $\{\kappa_1, \kappa_2\} = \{1.5, 0.9\}$. Red lines indicate $\bar{\gamma}_2 = 5$ dB whilst black lines indicate $\bar{\gamma}_2 = 1$ dB. Square markers represent average BEP obtained using approximate MGF expression.

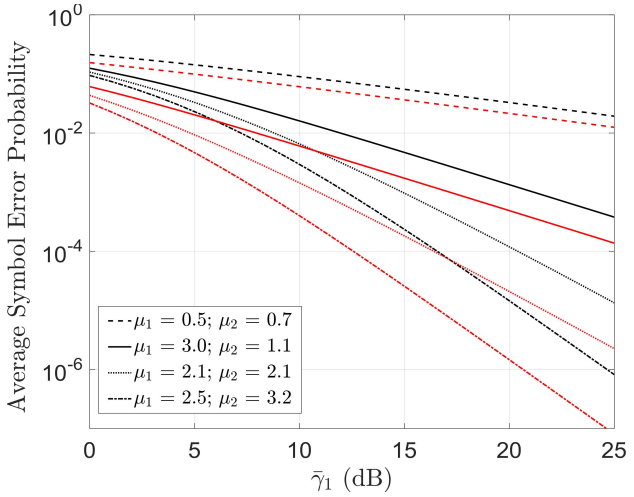

Fig. 9. Average SEP versus $\bar{\gamma}_1$ for a BPSK modulation scheme and for different values of μ_1 and μ_2. Here, $\bar{\gamma}_2 = 1, 5$ dB, and $\{\kappa_1, \kappa_2\} = \{1.5, 0.9\}$. Red lines indicate $\bar{\gamma}_2 = 5$ dB whilst black lines indicate $\bar{\gamma}_2 = 1$ dB.

VI. Applications

A. BAN Communications

To illustrate the utility of the new equations proposed here, we now analyze the outage probability for a dual-hop BAN system when each link undergoes κ-μ fading using channel data obtained from field trials. Exact details of the measurement setup, experiments, and data analysis can be found in [39]. Specifically, we consider the experiments that were performed in the reverberation chamber, and the scenario when both test subjects exhibited random movements within a circle of radius 0.5 m from their starting positions (see Fig. 10).

In [39], it was shown that the κ-μ PDF provided an excellent fit to the measured BAN channels. In this study, we consider the three node system shown in Fig. 10 to be representative of a dual-hop relay network, where Node's 1 and 2 are the source and the relay, respectively and Node 3 is the destination.

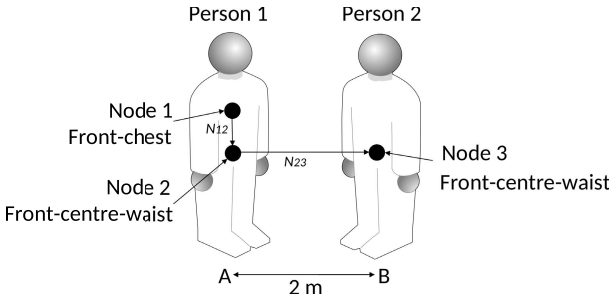

Fig. 10. On-body transceivers on front-chest of person 1 (Node 1), front-centre-waist of person 1 (Node 2) and front-centre-waist of person 2 (Node 3). N_{12} represents channel between the source node and the relay whilst N_{23} represents the channel between the relay and the destination node. In general, N_{XY} represents the channel between transmitter X and receiver Y. A and B denote the positions of the test subjects in the environment.

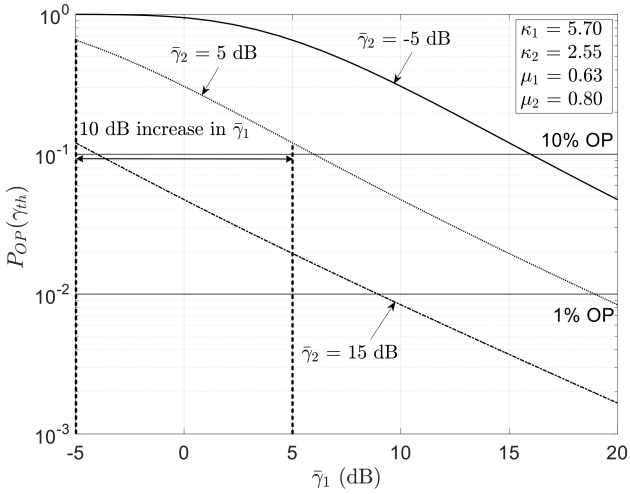

Fig. 11. Outage probability versus $\bar{\gamma}_1$ for BAN channel measurements in the reverberation chamber. Here, $\bar{\gamma}_{\text{th}} = 0$ dB.

Utilizing the parameter estimates from [39, Table I] we now provide some useful insights into the performance of BANs that are subject to double κ-μ fading,[2] as well as making some important recommendations on the thresholds that must be maintained to ensure adequate system performance. We perform our analysis when $\gamma_{\text{th}} = 0$ dB, $\bar{\gamma}_2 = 5$ dB and for $P_{\text{OP}}(\gamma_{\text{th}}) = 0.01$ (1% outage probability level) and 0.1 (10% outage probability level). Please note that these are representative of very low and relatively low outage probability levels.

Fig. 11 shows the outage probability versus $\bar{\gamma}_1$ in the reverberation chamber when both test subjects performed random movements. With $\bar{\gamma}_2$ fixed at 5 dB, we find that increasing $\bar{\gamma}_1$ from -5 dB to 5 dB causes the outage probability to significantly reduce from 0.65 to 0.12. Moreover, to ensure low outage probability levels of 10% and 1% for the dual-hop BAN system, we find that $\bar{\gamma}_1$ must always be greater than 6 dB and 18 dB, respectively.

[2]Since the channel from the source to the relay and relay to the destination follows the κ-μ distribution, the channel from the source to the destination can be viewed as a product of two κ-μ RVs.

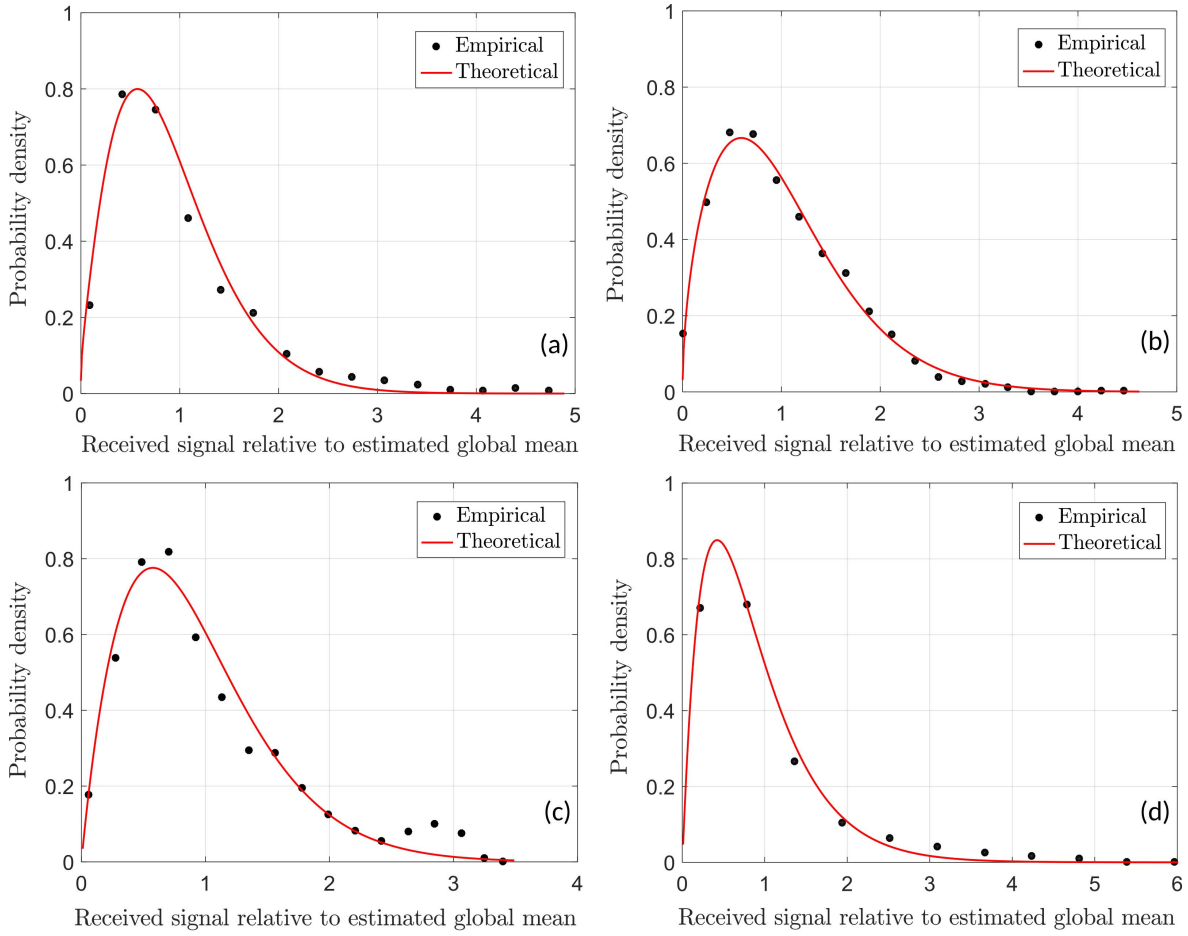

Fig. 12. Empirical (symbols) and theoretical (lines) PDFs of the κ-μ/κ-μ composite fading model fitted to the D2D channel measurements for (a) LOS indoor environment (b) NLOS indoor environment (c) LOS outdoor environment and (d) NLOS outdoor environment.

B. D2D Communications

In this subsection, we demonstrate a practical application of the κ-μ/κ-μ composite fading model by applying it to some D2D channel measurements. Specific details of the measurement hardware and experiments can be found in [40] and [41], respectively. The field measurements were obtained at 5.8 GHz within an indoor open office area and an outdoor open space environment. During the measurement trial (see [41, Fig. 1]), both persons had the hypothetical user equipment (UE) positioned at their heads. As well as this, person B had the UE in the right-front pocket of his clothing. The test subjects were initially stationary and then instructed to walk around randomly within a circle of radius 0.5 m from their starting position. Here, the head-to-head scenario indicates the Line of Sight (LOS) channel condition whilst the head-to-pocket scenario is representative of the non-line-of-sight (NLOS) channel condition.

For the analysis, the global mean signal power was removed from the D2D measurement data in order to obtain the composite fading signal. A minimum of 138148 samples of the received signal power were obtained and used for parameter estimation. As an example of the model fitting process, Fig. 12 shows the PDF of the κ-μ/κ-μ composite fading model fitted to the LOS and NLOS D2D channel measurements obtained for the indoor and outdoor environments, respectively. All parameter estimates were obtained using the `lsqnonlin` function available in the optimization toolbox of Matlab along with the κ-μ/κ-μ composite fading PDF. To compute the estimates, a set of lower and upper bounds for the κ-μ/κ-μ composite fading parameters are first defined, and then some initial starting points for the parameters are chosen randomly and input into the Matlab function. The function then uses the Trust-Region-Reflective least squares algorithm [42], [43] to obtain the optimal parameter estimates.

From Fig. 12, the utility of the κ-μ/κ-μ composite model for modeling D2D channels which occur in both indoor and outdoor environments can be clearly identified. In three of the four cases considered (Figs. 12(a), (b) and (d)), the empirical and theoretical PDFs are in very good agreement, with only a slight disparity noticed at the upper tail of the PDFs given in Figs. 12(a) and (d). In Fig. 12(c), while the theoretical κ-μ/κ-μ composite PDF provided a good approximation of the empirical data, there are a number of identifiable points for which this approximation is less satisfactory. These can be identified around the mode, median and upper tail of the empirical PDF suggesting that in the case of LOS D2D communications which occur in an outdoor environment, the κ-μ/κ-μ composite model alone may not be sufficient to

TABLE III

PARAMETER ESTIMATES FOR THE κ-μ/κ-μ COMPOSITE FADING MODEL FITTED TO THE D2D MEASURED DATA

Environments	Channel type	κ-μ/κ-μ composite model				
		κ_1	μ_1	κ_2	μ_2	$\bar{r}_2$
Indoor	LOS	3.94	0.67	0.72	1.18	0.89
	NLOS	0.78	1.92	1.00	0.75	1.02
Outdoor	LOS	1.41	1.08	1.00	1.14	0.93
	NLOS	0.01	1.18	0.02	1.17	0.87

characterize the propagation mechanisms which are responsible for shaping the fading that is observed. To allow the reader to reproduce these plots, parameter estimates for all of the D2D measurement scenarios are given in Table III.

From Table III, for the LOS channel condition we observe that the parameter estimates for κ_1 are larger than 1, indicating that these channels are strongly influenced by dominant signal components. However, this is not true for the NLOS channel condition where $\kappa_1 < 1$ were observed. For both environments, the κ_2 estimates for the LOS channel condition were observed to be quite low, suggesting that the LOS link was subject to some shadowing. Partial obstruction of the dominant signal components caused by test subjects performing random movements was most likely responsible for this observation. Furthermore, we observe that both the μ_1 and μ_2 estimates are close to 1, suggesting that a single cluster of scattered multipath contribute to the signals received in both the indoor and outdoor environments.

VII. CONCLUSION

In this paper, novel analytical expressions are derived for the PDF, CDF and MGF of the product of two κ-μ RVs. Specifically, analytical expressions have been obtained for *i.n.i.d* channel coefficients without any restrictions on the parameters. Approximate closed-form expressions have also been presented that agree well with the analytical expressions and Monte-Carlo simulations. Utilizing these results, closed-form formulations are obtained for the higher order moments, and performance metrics such as the AF and CQEI. Additionally, analytical expressions are obtained for the outage probability, ACC, average SEP and average BEP for the double κ-μ fading channel. These formulations are very flexible and include as special cases a variety of double fading models currently available in the literature. The utility of the new formulations has been illustrated by investigating the outage probability of a dual-hop BAN system when each link experiences κ-μ fading using data obtained from real channel measurements. The statistics of the κ-μ/κ-μ composite fading channel can be obtained as a byproduct of the formulations presented here. To this end, a practical application of the κ-μ/κ-μ composite fading model has been demonstrated by applying it to D2D channel measurements. Finally, we see that the analytical results presented in this paper compute efficiently, and can easily be evaluated in Mathematica.

APPENDIX A
PROOF OF EQUATION (9)

Substituting $G_{0,2}^{2,0}(z|_{b,\,c}) = 2z^{\frac{1}{2}(b+c)}\mathrm{K}_{b-c}\left(2\sqrt{z}\right)$ [38, 07.34.03.0605.01] in (7), where $\mathrm{K}_\phi(\cdot)$ is the ϕth-order modified Bessel function of the second kind, we obtain

$$f_X(x) = \frac{2}{\rho_{1,2}}\sum_{m=0}^{\infty}\sum_{n=0}^{\infty}\frac{(\kappa_1\mu_1)^m(\kappa_2\mu_2)^n(\theta_1\theta_2)^{\frac{\xi}{2}}}{m!n!\Gamma(m+\mu_1)\Gamma(n+\mu_2)} \times x^{\frac{1}{2}(-2+\xi)}\,\mathrm{K}_{m-n+\mu_1-\mu_2}\left(2\sqrt{\frac{x}{\mathcal{K}_1\mathcal{K}_2}}\right) \quad (29)$$

where $\rho_{1,2}=\mathrm{e}^{\mu_1\kappa_1+\mu_2\kappa_2}$, $\mathcal{K}_1=\frac{1}{\theta_1}$, $\mathcal{K}_2=\frac{1}{\theta_2}$ and $\xi=m+n+\mu_1+\mu_2$. Now changing the order of summation, followed by changing the index m to $j+n$ we obtain

$$f_X(x) = \frac{2}{\rho_{1,2}}\sum_{n=0}^{\infty}\sum_{j=-n}^{\infty}\frac{(\kappa_1\mu_1)^{j+n}(\kappa_2\mu_2)^n(\theta_1\theta_2)^{\frac{\xi_1}{2}}}{n!(j+n)!\Gamma(j+n+\mu_1)\Gamma(n+\mu_2)} \times x^{\frac{1}{2}(-2+\xi_1)}\mathrm{K}_{j+\mu_1-\mu_2}\left(2\sqrt{\frac{x}{\mathcal{K}_1\mathcal{K}_2}}\right) \quad (30)$$

where $\xi_1=j+2n+\mu_1+\mu_2$.

Expressing the inner series in (30) as $\sum_{j=-n}^{\infty}a_j = \sum_{j=-n}^{-1}a_j+\sum_{j=0}^{\infty}a_j$, we obtain (31), as shown on the top of the next page. Now changing the index, $j=j-n$ in the first summation we have (32), as shown on the top of the next page, where $\xi_2=j+n+\mu_1+\mu_2$.

Rewriting the inner series in (32), as $\sum_{j=0}^{n-1}a_j = \sum_{j=0}^{n}a_j - a_n$, followed by expressing the first and the last sum in terms of the regularized Hypergeometric function [32], we obtain (33), as shown on the top of the next page, where $\zeta_1=\frac{x\kappa_1\kappa_2\mu_1\mu_2}{\mathcal{K}_1\mathcal{K}_2}$ and $\xi_3=j+\mu_1+\mu_2$.

Following a similar simplification approach as above for the double summation in (33), as shown at the top of the next page, changing the index $n=n+j$, summing over index n, and finally performing some algebraic manipulations we obtain the PDF of the double κ-μ fading channel shown in (9), which completes the proof.

APPENDIX B
PROOF OF EQUATION (14)

Substituting (7) in (13), we obtain

$$\mathbb{E}\left[\mathrm{e}^{-sX}\right] = \frac{\theta_1\theta_2}{\rho_{1,2}}\sum_{m=0}^{\infty}\sum_{n=0}^{\infty}c_{n,m} \times \underbrace{\int_0^{\infty}\mathrm{e}^{-sx}G_{0,2}^{2,0}\left(x\;\theta_1\theta_2\middle|\;{}_{m+\mu_1-1,n+\mu_2-1}\right)\mathrm{d}x}_{\triangleq I_1} \quad (34)$$

where the integral I_1 can be simplified by using [28, eq. 7.811.4] and [38, 07.34.21.0011.01] as

$$I_1 = \int_0^{\infty}G_{0,1}^{1,0}\left(sx\middle|\;{}_{0}\right)G_{0,2}^{2,0}\left(x\;\theta_1\theta_2\middle|\;{}_{n+\mu_1-1,\;m+\mu_2-1}\right)\mathrm{d}x = \frac{1}{\theta_1\theta_2}G_{2,1}^{1,2}\left(\frac{s}{\theta_1\theta_2}\middle|\;{}_{0}^{1-n-\mu_1,\;1-m-\mu_2}\right). \quad (35)$$

$$f_X(x) = \frac{2}{\rho_{1,2}} \sum_{n=0}^{\infty} \Bigg[\sum_{j=-n}^{-1} \frac{(\kappa_1\mu_1)^{j+n} (\kappa_2\mu_2)^n \, (\theta_1\theta_2)^{\frac{\xi_1}{2}}}{n!\,(j+n)!\Gamma(j+n+\mu_1)\Gamma(n+\mu_2)} x^{\frac{1}{2}(-2+\xi_1)} \mathrm{K}_{j+\mu_1-\mu_2}\left(2\sqrt{\frac{x}{\mathcal{K}_1\mathcal{K}_2}}\right) + \sum_{j=0}^{\infty} \frac{(\kappa_1\mu_1)^{j+n} (\kappa_2\mu_2)^n \, (\theta_1\theta_2)^{\frac{\xi_1}{2}}}{n!(j+n)!\Gamma(j+n+\mu_1)\Gamma(n+\mu_2)} x^{\frac{1}{2}(-2+\xi_1)} \mathrm{K}_{j+\mu_1-\mu_2}\left(2\sqrt{\frac{x}{\mathcal{K}_1\mathcal{K}_2}}\right) \Bigg]. \tag{31}$$

$$f_X(x) = \frac{2}{\rho_{1,2}} \sum_{n=0}^{\infty} \Bigg[\sum_{j=0}^{n-1} \frac{(\kappa_1\mu_1)^{j} (\kappa_2\mu_2)^n (\theta_1\theta_2)^{\frac{\xi_2}{2}}}{n!j!\Gamma(j+\mu_1)\Gamma(n+\mu_2)} x^{\frac{1}{2}(-2+\xi_2)} \mathrm{K}_{j-n+\mu_1-\mu_2}\left(2\sqrt{\frac{x}{\mathcal{K}_1\mathcal{K}_2}}\right) + \sum_{j=0}^{\infty} \frac{(\kappa_1\mu_1)^{j+n} (\kappa_2\mu_2)^n (\theta_1\theta_2)^{\frac{\xi_1}{2}}}{n!(j+n)!\Gamma(j+n+\mu_1)\Gamma(n+\mu_2)} x^{\frac{1}{2}(-2+\xi_1)} \mathrm{K}_{j+\mu_1-\mu_2}\left(2\sqrt{\frac{x}{\mathcal{K}_1\mathcal{K}_2}}\right) \Bigg]. \tag{32}$$

$$\begin{aligned} f_X(x) = {} & \frac{-2\,(\theta_1\theta_2)^{\frac{\mu_1}{2}+\frac{\mu_2}{2}}}{\rho_{1,2}} x^{-1+\frac{\mu_1}{2}+\frac{\mu_2}{2}} \mathrm{K}_{\mu_1-\mu_2}\left(2\sqrt{\frac{x}{\mathcal{K}_1\mathcal{K}_2}}\right) {}_0\widetilde{F}_3\,(;1,\mu_1,\mu_2;\zeta_1) \\ & + \frac{2}{\rho_{1,2}} \sum_{n=0}^{\infty} \sum_{j=0}^{n} \frac{(\kappa_1\mu_1)^{j} (\kappa_2\mu_2)^n (\theta_1\theta_2)^{\frac{\xi_2}{2}}}{n!j!\Gamma(j+\mu_1)\Gamma(n+\mu_2)} x^{\frac{1}{2}(-2+\xi_2)} \mathrm{K}_{j-n+\mu_1-\mu_2}\left(2\sqrt{\frac{x}{\mathcal{K}_1\mathcal{K}_2}}\right) \\ & + \frac{2}{\rho_{1,2}} \sum_{j=0}^{\infty} (\kappa_1\mu_1)^{j} (\theta_1\theta_2)^{\frac{\xi_3}{2}} x^{-1+\frac{\xi_3}{2}} \mathrm{K}_{j+\mu_1-\mu_2}\left(2\sqrt{\frac{x}{\mathcal{K}_1\mathcal{K}_2}}\right) {}_0\widetilde{F}_3\,(;1+j,j+\mu_1,\mu_2;\zeta_1)\,. \end{aligned} \tag{33}$$

Now substituting (35) in (34) and using [38, 07.34.03.0392.01] to rewrite the Meijer-G term in the form of confluent Tricomi hypergeometric function we obtain (14), which completes the proof.

Appendix C
Proof of Equation (17)

Substituting $q = 1$ and 2 in (15), followed by using the transformation ${}_1F_1\,(a;b;z) = \mathrm{e}^z {}_1F_1\,(b-a;b;-z)$ [38, 07.20.16.0001.01] and replacing the confluent hypergeometric function with its series form [38, 07.20.02.0001.01], $\mathbb{E}[X]$ and $\mathbb{E}\left[X^2\right]$ simplify to

$$\mathbb{E}[X] = \bar{\gamma_1}\bar{\gamma_2} \tag{36}$$

and

$$\mathbb{E}\left[X^2\right] = \frac{\mu_1\,(1+\mu_1)\,\mu_2\,(1+\mu_2)}{\theta_1^2\theta_2^2} \left[1+\kappa_1\left(2+\frac{\kappa_1\mu_1}{1+\mu_1}\right)\right] \times \left[1+\kappa_2\left(2+\frac{\kappa_2\mu_2}{1+\mu_2}\right)\right]. \tag{37}$$

Now substituting (36) and (37) in (16), followed by performing some basic mathematical manipulations we obtain (17), which completes the proof.

Appendix D
Proof of Equation (22)

Substituting (7) in (21), we obtain

$$\frac{C}{W} = \frac{\log_2\mathrm{e}\;\theta_1\theta_2}{\rho_{1,2}} \sum_{m=0}^{\infty}\sum_{n=0}^{\infty} c_{n,m} \times \underbrace{\int_0^{\infty} \log_{\mathrm{e}}(1+x)\, G_{0,2}^{2,0}\left(x\;\theta_1\theta_2\middle|\; m+\mu_1-1, n+\mu_2-1\right) \mathrm{d}x}_{\triangleq I_2} \tag{38}$$

where the integral I_2 can be simplified by using [38, 01.04.26.0003.01] and [28, eq. 7.811.1] as

$$\begin{aligned} I_2 &= \int_0^{\infty} G_{2,2}^{1,2}\left(x\middle|\begin{matrix}1,\;1\\1,\;0\end{matrix}\right) G_{0,2}^{2,0}\left(x\;\theta_1\theta_2\middle|\; n+\mu_1-1,\; m+\mu_2-1\right) \mathrm{d}x \\ &= G_{2,4}^{4,1}\left(\theta_1\theta_2\middle|\begin{matrix}-1,\;0\\-1,\;-1,\;m+\mu_1-1,\;n+\mu_2-1\end{matrix}\right). \end{aligned} \tag{39}$$

Now substituting (39) in (38) we obtain (22), which completes the proof.

References

[1] D. Tse and P. Viswanath, *Fundamentals of Wireless Communication*, 1st ed. Cambridge, U.K: Cambridge Univ. Press, 2005.

[2] N. Fasarakis-Hilliard, P. N. Alevizos, and A. Bletsas, "Coherent detection and channel coding for bistatic scatter radio sensor networking," *IEEE Trans. Commun.*, vol. 63, no. 5, pp. 1798–1810, May 2015.

[3] C. Boyer and S. Roy, "Backscatter communication and RFID: Coding, energy, and MIMO analysis," *IEEE Trans. Commun.*, vol. 62, no. 3, pp. 770–785, Mar. 2014.

[4] P. N. Alevizos, A. Bletsas, and G. N. Karystinos, "Noncoherent short packet detection and decoding for scatter radio sensor networking," *IEEE Trans. Commun.*, vol. 65, no. 5, pp. 2128–2140, May 2017.

[5] P. N. Alevizos, K. Tountas, and A. Bletsas. (Jun. 2017). "Multistatic scatter radio sensor networks for extended coverage." [Online]. Available: https://arxiv.org/abs/1706.03091

[6] B. Talha and M. Pätzold, "Channel models for mobile-to-mobile cooperative communication systems: A state of the art review," *IEEE Veh. Technol. Mag.*, vol. 6, no. 2, pp. 33–43, Jun. 2011.

[7] V. Erceg, S. J. Fortune, J. Ling, A. J. Rustako, and R. A. Valenzuela, "Comparisons of a computer-based propagation prediction tool with experimental data collected in urban microcellular environments," *IEEE J. Sel. Areas Commun.*, vol. 15, no. 4, pp. 677–684, May 1997.

[8] T. Taniguchi, Y. Karasawa, and M. Tsuruta, "An analysis method of double fading MIMO channels including LOS environments," in *Proc. IEEE 19th Int. Symp. Pers., Indoor Mobile Radio Commun.*, Cannes, France, Sep. 2008, pp. 1–5.

[9] D. Chizhik, G. J. Foschini, and R. A. Valenzuela, "Capacities of multi-element transmit and receive antennas: Correlations and keyholes," *Electron. Lett.*, vol. 36, no. 13, pp. 1099–1100, Jun. 2000.

[10] H. Shin and J. H. Lee, "Performance analysis of space-time block codes over keyhole Nakagami-*m* fading channels," *IEEE Trans. Veh. Technol.*, vol. 53, no. 2, pp. 351–362, Mar. 2004.

[11] D. W. Matolak and J. Frolik, "Worse-than-Rayleigh fading: Experimental results and theoretical models," *IEEE Commun. Mag.*, vol. 49, no. 4, pp. 140–146, Apr. 2011.

[12] E. Bayaki, R. Schober, and R. K. Mallik, "Performance analysis of MIMO free-space optical systems in gamma-gamma fading," *IEEE Trans. Commun.*, vol. 57, no. 11, pp. 3415–3424, Nov. 2009.

[13] M. A. Al-Habash, L. C. Andrews, and R. L. Phillips, "Mathematical model for the irradiance probability density function of a laser beam propagating through turbulent media," *Opt. Eng.*, vol. 40, pp. 1554–1562, Aug. 2001.

[14] J. Salo, H. M. El-Sallabi, and P. Vainikainen, "Statistical analysis of the multiple scattering radio channel," *IEEE Trans. Antennas Propag.*, vol. 54, no. 11, pp. 3114–3124, Nov. 2006.

[15] G. K. Karagiannidis, N. C. Sagias, and P. T. Mathiopoulos, "N^*Nakagami: A novel stochastic model for cascaded fading channels," *IEEE Trans. Commun.*, vol. 55, no. 8, pp. 1453–1458, Aug. 2007.

[16] E. J. Leonardo and M. D. Yacoub, "The product of two α-μ variates and the composite α-μ multipath–shadowing model," *IEEE Trans. Veh. Technol.*, vol. 64, no. 6, pp. 2720–2725, Jun. 2015.

[17] M. K. Simon and M.-S. Alouini, *Digital Communication Over Fading Channels*, 2nd ed. New York, NY, USA: Wiley, 2005.

[18] M. D. Yacoub, "The κ-μ distribution and the η-μ distribution," *IEEE Antennas Propag. Mag.*, vol. 49, no. 1, pp. 68–81, Feb. 2007.

[19] M. S. Alouini and M. K. Simon, "Dual diversity over correlated log-normal fading channels," *IEEE Trans. Commun.*, vol. 50, no. 12, pp. 1946–1959, Dec. 2002.

[20] A. Abdi and M. Kaveh, "On the utility of gamma PDF in modeling shadow fading (slow fading)," in *Proc. IEEE Veh. Technol. Conf.*, Houston, TX, USA, May 1999, pp. 2308–2312.

[21] S. L. Cotton and W. G. Scanlon, "An experimental investigation into the influence of user state and environment on fading characteristics in wireless body area networks at 2.45 GHz," *IEEE Trans. Wireless Commun.*, vol. 8, no. 1, pp. 6–12, Jan. 2009.

[22] S. L. Cotton, "Human body shadowing in cellular device-to-device communications: Channel modeling using the shadowed κ-μ fading model," *IEEE J. Sel. Areas Commun.*, vol. 33, no. 1, pp. 111–119, Jan. 2015.

[23] S. K. Yoo, N. Bhargav, S. L. Cotton, P. C. Sofotasios, M. Matthaiou, M. Valkama, and G. K. Karagiannidis, "The κ-μ/inverse gamma and η-μ/inverse gamma composite fading models: Fundamental statistics and empirical validation," *IEEE Trans. Commun.*, to be published.

[24] A. Abdi and M. Kaveh, "K distribution: An appropriate substitute for Rayleigh–lognormal distribution in fading-shadowing wireless channels," *Electron. Lett.*, vol. 34, no. 9, pp. 851–852, Apr. 1998.

[25] E. Jakeman and R. J. A. Tough, "Generalized K distribution: A statistical model for weak scattering," *J. Opt. Soc. Amer.*, vol. 4, no. 9, pp. 1764–1772, Sep. 1987.

[26] N. Bhargav, S. L. Cotton, and D. B. Smith, "An experimental-based analysis of inter-BAN co-channel interference using the κ-μ fading model," *IEEE Trans. Antennas Propag.*, vol. 65, no. 2, pp. 983–988, Feb. 2017.

[27] C. R. N. da Silva, E. J. Leonardo, and M. D. Yacoub, "Product of two envelopes taken from α-μ, κ-μ, and η-μ distributions," *IEEE Trans. Commun.*, to be published.

[28] I. S. Gradshteyn and I. M. Ryzhik, *Table of Integrals, Series, and Products*, 7th ed. New York, NY, USA: Academic, 2007.

[29] M. Abramowitz and I. A. Stegun, *Handbook of Mathematical Functions*. Washington, DC, USA: U.S. Dept. of Commerce, National Bureau of Standards, 1972.

[30] S. Nadarajah, "Exact distribution of the product of m gamma and n Pareto random variables," *J. Comput. Appl. Math.*, vol. 235, no. 15, pp. 4496–4512, Jun. 2011.

[31] V. S. Adamchik and O. I. Marichev, "The algorithm for calculating integrals of hypergeometric type functions and its realization in REDUCE system," in *Proc. Int. Symp. Symbolic Algebraic Comput.*, Tokyo, Japan, 1990, pp. 212–224.

[32] E. W. Weisstein. (2017). *Regularized Hypergeometric Function*. Accessed: Feb. 27, 2017. [Online]. Available: http://mathworld.wolfram.com/RegularizedHypergeometricFunction

[33] A. S. Lioumpas, G. K. Karagiannidis, and A. C. Iossifides, "Channel quality estimation index (CQEI): An improved performance criterion for wireless communications systems over fading channels," in *Proc. 12th Eur. Wireless Conf.-Enabling Technol. Wireless Multimedia Commun.*, Athens, Greece, Apr. 2006, pp. 1–6.

[34] D. B. Da Costa and M. D. Yacoub, "Average channel capacity for generalized fading scenarios," *IEEE Commun. Lett.*, vol. 11, no. 12, pp. 949–951, Dec. 2007.

[35] A. J. Goldsmith, *Wireless Communications*. Cambridge, U.K: Cambridge Univ. Press, 2005.

[36] L.-L. Li, F. Li, and F. B. Gross, "A new polynomial approximation for J_v Bessel functions," *Appl. Math. Comput.*, vol. 183, no. 2, pp. 1220–1225, Dec. 2006.

[37] M. K. Simon, *Probability Distributions Involving Gaussian Random Variables: A Handbook for Engineers, Scientists and Mathematicians*. Secaucus, NJ, USA: Springer-Verlag, 2006.

[38] Wolfram Research, Inc. (2016). *Wolfram Research*. Accessed: Nov. 9, 2016. [Online]. Available: http://functions.wolfram.com/id

[39] N. Bhargav, S. L. Cotton, G. A. Conway, A. McKernan, and W. G. Scanlon, "Simultaneous channel measurements of the on-body and body-to-body channels," in *Proc. IEEE 27th Annu. Int. Symp. Pers., Indoor, Mobile Radio Commun.*, Valencia, Spain, Sep. 2016, pp. 1–6.

[40] N. Bhargav, S. L. Cotton, and D. E. Simmons, "Secrecy capacity analysis over κ–μ fading channels: Theory and applications," *IEEE Trans. Commun.*, vol. 64, no. 7, pp. 3011–3024, Jul. 2016.

[41] S. K. Yoo, S. L. Cotton, P. C. Sofotasios, M. Matthaiou, M. Valkama, and G. K. Karagiannidis, "The Fisher–Snedecor F distribution: A simple and accurate composite fading model," *IEEE Commun. Lett.*, vol. 21, no. 7, pp. 1661–1664, Jul. 2017.

[42] J. E. Dennis, "Nonlinear least squares and equations," in *The State of the Art in Numerical Analysis*, D. Jacobs, Ed. New York, NY, USA: Academic, 1977.

[43] J. J. Moré and D. C. Sorensen, "Computing a trust region step," *SIAM J. Sci. Statist. Comput.*, vol. 4, no. 3, pp. 553–572, Sep. 1983.

Nidhi Bhargav (S'15) received the B.E. degree (Hons.) in telecommunications engineering from Visvesvaraya Technological University, Belgaum, India, in 2011, and the M.Sc. degree (Hons.) in wireless communications and signal processing from the University of Bristol, U.K., in 2012. She is currently pursuing the Ph.D. degree with the Queen's University of Belfast, U.K. Her research interests include physical-layer security, channel characterization and modeling, and cellular device-to-device and body-centric communications.

Carlos Rafael Nogueira da Silva was born in Brazil in 1986. He received the B.S. degree in electrical engineering from the Federal University of Itajubá, Itajubá, Brazil, in 2010, and the M.S. degree in electrical engineering from the National Institute of Telecommunications, Santa Rita do Sapucaí, Brazil, in 2012. He is currently pursuing the Ph.D. degree with the School of Electrical and Computer Engineering, University of Campinas. His research interests include wireless channel modeling, spectrum sensing, cognitive radio, and wireless communications in general.

Young Jin Chun (M'12) received the B.S. degree from Yonsei University, Seoul, South Korea, in 2004, the M.S. degree from the University of Michigan, Ann Arbor, MI, USA, in 2007, and the Ph.D. degree from Iowa State University, Ames, IA, USA, in 2011, all in electrical engineering. He was a Post-Doctoral Researcher with Sungkyunkwan University, Suwon, South Korea, from 2011 to 2012, and with Qatar University, Doha, Qatar, from 2013 to 2014. In 2015, he joined Queen's University Belfast, U.K., as a Research Fellow. His research interests are primarily in the area of wireless communications with emphasis on stochastic geometry, system-level network analysis, device-to-device communications, and the various use cases of 5G communications.

Élvio João Leonardo was born and grew up in Brazil. He received the B.Eng., M.Sc., and Ph.D. degrees in electrical engineering from the University of Campinas, Brazil, in 1984, 1992, and 2013, respectively. He was involved in the development of telecommunications equipment at the Telebras Research and Development Centre. In 1992, he moved to Australia, where he was with The University of Sydney. In 1995, he joined the Software Centre, Motorola, Adelaide, SA, Australia, where he was involved in projects in the communications area. In 1998, still with Motorola, he moved to Chicago, where he spent the next four years. He decided to move back to Brazil, where he started his academic career. He is currently an Adjunct Professor with the State University of Maringá. His research interests include wireless communications and embedded systems.

Simon L. Cotton (S'04–M'07–SM'14) received the B.Eng. degree in electronics and software from the University of Ulster, Ulster, U.K., in 2004, and the Ph.D. degree in electrical and electronic engineering from the Queen's University of Belfast, Belfast, U.K., in 2007. He is currently a Reader in wireless communications with the Institute of Electronics, Communications and Information Technology, Queen's University Belfast. He is also a Co-Founder and the Chief Technology Officer with ActivWireless Ltd., Belfast, U.K. He has authored and co-authored over 100 publications in major the IEEE/IET journals and refereed international conferences and two book chapters. He holds two patents. Among his research interests are cellular device-to-device, vehicular, and wearable communications. His other research interests include radio channel characterization and modeling and the simulation of wireless channels. In 2010, he received the H. A. Wheeler Prize from the IEEE Antennas and Propagation Society for the best applications journal paper in the IEEE TRANSACTIONS ON ANTENNAS AND PROPAGATION in 2009. In 2011, he received the Sir George Macfarlane Award from the U.K. Royal Academy of Engineering in recognition of his technical and scientific attainment since graduating from his first degree in engineering.

Michel Daoud Yacoub (M'05) was born in Brazil in 1955. He received the B.S.E.E. and M.Sc. degrees from the School of Electrical and Computer Engineering, University of Campinas (UNICAMP), Campinas, Brazil, in 1978 and 1983, respectively, and the Ph.D. degree from the University of Essex, U.K., in 1988. From 1978 to 1985, he was a Research Specialist in the development of the Tropico digital exchange family with the Research and Development Center of Telebrás, Brazil. In 1989, he joined the School of Electrical and Computer Engineering, UNICAMP, where he is currently a Full Professor. He consults for several operating companies and industries in the wireless communications area. He is the author of the *Foundations of Mobile Radio Engineering* (Boca Raton, FL, USA: CRC, 1993) and *Wireless Technology: Protocols, Standards, and Techniques* (Boca Raton, FL, USA: CRC, 2001), and the co-author of *Telecommunications: Principles and Trends* (São Paulo, Brazil: Erica, 1997, in Portuguese). He holds two patents. His general research interests include wireless communications.